Meteorins regulate the formation of the left-right organizer and the establishment of vertebrate body asymmetry

Fanny Eggeler[1], Jonathan Boulanger-Weill[1], Flavia De Santis[2,‡], Laura Belleri[1], Karine Duroure[1], Thomas O. Auer[2,#], Shahad Albadri[1*], Filippo Del Bene[1*]

[1] Sorbonne Université, INSERM, CNRS, Institut de la Vision, F-75012 Paris, France

[2] Institut Curie, PSL Research University, Inserm U934, CNRS UMR3215, Paris, France

‡ Present Address: ZeClinics SL, Badalona, Spain

Present Address: Center for Integrative Genomics, Faculty of Biology and Medicine, University of Lausanne, CH-1015 Lausanne, Switzerland

* For correspondence: shahad.albadri@inserm.fr; filippo.del-bene@inserm.fr

ABSTRACT

The body plan of vertebrates appears externally bilaterally symmetric. Nonetheless the positioning and morphology of internal organs often display a strict left-right (L-R) asymmetry that is essential for their functions. During vertebrate embryonic development left-right symmetry-breaking is innated by a ciliated organ called the Node or left-right organizer. Within the Node, a leftward flow of extraembryonic fluid named the Nodal flow mediates the asymmetric expressions of Nodal factors. Although downstream Nodal pathway components leading to the establishment of the embryonic left-right axis are well known, less is known about the development and formation of the embryonic Node itself.

Here we reveal a novel role for the Meteorin protein family in the establishment of the left-right axis and in the formation of the Kupffer's vesicle, the Node equivalent structure in zebrafish. We show that the genetic inactivation of each or all three members of the zebrafish Meteorin family (*metrn*, *metrn-like 1* and *metrn-like 2*) leads to defects in properties of the Kupffer's vesicle, caused by impaired assembly and migration of the Kupffer's vesicle forming dorsal forerunner cells. In addition, we demonstrate that Meteorins genetically interact with integrins ItgαV and Itgβ1b regulating the dorsal forerunner cell clustering and that *meteorins* loss-of-function results in disturbed Nodal factor expression and consequently in randomized or symmetric heart looping and jogging.

These results identify a new role for the Meteorin protein family in the left-right asymmetry patterning during embryonic vertebrate development.

INTRODUCTION

From the outside the vertebrate body plan appears bilaterally symmetric. However, internal organs positioning and morphology often displays left-right (L-R) asymmetries. For instance, in vertebrates the heart generally lies on the left side, the liver and the pancreas are positioned on the right and the gut presents asymmetric rotations.

One major regulator for the establishment of the L-R axis is Nodal, a ligand belonging to the TGFβ protein family [1]–[6]. Its signaling is activated in the left lateral plate mesoderm (LPM), whereas Nodal remains inactive in the right LPM, creating an embryo-scale left-right asymmetry [3]. In mice, this asymmetry is achieved by an oriented rotation of the cilia of a structure called the Node generating a leftward flow of extraembryonic fluid named the Nodal flow. This results in an asymmetric expression of several Nodal factors and Nodal signaling. Participating in this patterning, Leftys, soluble inhibitors belonging to a subclass of TGF factors, antagonize Nodal signaling [7], [8].
The Node and the Nodal flow were shown to be conserved in numerous vertebrates. In chicken it is known as the Hensen's node, in Xenopus the gastrocoel roof plate and in zebrafish the Kupffer's vesicle (KV) [9]–[15] and all are key points of the L-R symmetry breaking during the embryonic development [12], [14], [16].

Compared to the relatively flat shaped mouse node, the zebrafish KV is a fluid-filled sphere with a ciliated epithelium and it is formed by dorsal forerunner cells (DFCs) [9]. DFCs first emerge as cells of the epithelium of the dorsal surface in direct contact with the yolk syncytial layer at 6 hours post-fertilization (hpf) [17]. Around 8 to 9 hpf, following the epibolic movement, 20 to 30 DFCs form a single cluster and migrate towards the vegetal pole in a non-involuting manner at the leading edge of the shield. During this migration process, polarized DFCs organize into multiple focal points by retaining long-lasting apical contacts within the cluster and remaining delaminated DFCs maintain contact with the cluster by cell-cell contact mechanisms. At the final phase of epiboly and after reaching the vegetal pole, the DFC cluster is separating from the dorsal marginal enveloping layer cells by losing the apical contacts. The focal points of the cluster are then rearranged by integrating the unpolarized DFCs to form a single focal point that will expand into a monolayer rosette structure containing a lumen to form the KV by 12 hpf [9], [17], [18]. Along this process, non-motile and motile monocilia are generated on the apical membrane facing the lumen that create a counterclockwise flow of fluid by the KV, called Nodal flow. It was shown that the leftward directed flow within the KV results in asymmetric expression of zebrafish Nodal genes, like *spaw*, *lefty1* and *lefty2* that is

fundamental for proper L-R pattering [19], [20]. However, the molecular mechanisms involved in correct DFC migration and clustering that will form the KV remain largely elusive.

In this context, it has been reported that *nodal, lefty* as well as *p-smad2* expression are downregulated in *Meteorin*-null ES-cells. As such, Meteorin (Metrn) was hypothesized to be a novel important regulator of Nodal transcription [21].

Meteorin (Metrn), a secreted neurotrophic factor highly conserved among vertebrates, is expressed during early mouse development and is already detected at the blastocyst stage in the inner cell mass and then expands through the extraembryonic ectoderm to the central (CNS) and peripheral nervous system (PNS) during later developmental stages [21]. It was first described to induce glial cells differentiation and to promote axonal extension in dorsal root ganglion (DRG) explants *in vitro* [22]. Also conserved among vertebrates, its paralog Meteorin-like (Metrnl) has been first reported as a downstream target of the Pax2/5/8 signaling pathway during otic vesicle development [23] and was later shown to have neurotrophic properties comparable to the ones of Metrn [24]. The disruption of *Metrn* resulted in early embryonic lethality [21] preventing to investigate the role of Metrn proteins in early embryonic development *in vivo* and in particular its role in L-R patterning.

Here, using the zebrafish larva as model system, we generated knockout lines for all three-existing zebrafish *metrn* genes (*metrn*, *metrnl1* and *metrnl2*). All three single mutants are viable but we detect organ patterning defects with randomized or symmetric heart looping in *metrns* mutant embryos. Like in mouse, *metrn* genes are expressed during early development already from the 2-cells stage and transcripts are present in DFCs as well as in the KV structure. *Metrns* loss of function leads to DFC disorganization and Nodal flow formation defects within the KV. Together our study reveals a critical role for Metrn proteins in the DFC clustering and KV formation and in the establishment of the L-R axis.

RESULTS

Metrns loss-of-function affects proper heart looping and correct visceral organs positioning

To study the functions of Meteorin proteins during early development, we generated knock out zebrafish lines using the CRISPR/Cas9 technology to target the second exon of each gene that encodes for the signal peptide sequence. The newly generated zebrafish mutant lines carried out-of-frame deletions in the coding sequence of *metrn*, *metrnl1* and *metrnl2* (Supplementary Fig. 1A). In contrast to published embryonic lethal *Metrn* mouse mutants [21], constitutive homozygote mutants for all three genes individually (*metrn*$^{-/-}$; *metrnl1*$^{-/-}$; *metrnl2*$^{-/-}$), in double (*metrn*$^{-/-}$, *metrnl1*$^{-/-}$; *metrn*$^{-/-}$, *metrnl2*$^{-/-}$; *metrnl1*$^{-/-}$, *metrnl2*$^{-/-}$) and triple (*metrn*$^{-/-}$, *metrnl1*$^{-/-}$, *metrnl2*$^{-/-}$ or triplMut) mutant zebrafish were all viable and did not show any obvious morphological defects (Fig. 1A). We first validated that our mutagenic approach resulted in the generation of null alleles. To do so, we compared the expression level of all three *metrn* genes upon total mRNA extraction from 14 and 48 hpf WT and triplMut embryos by qRT-PCR. *Metrn* and *metrnl1* expression was detected in samples of 14 hpf WT embryos and *metrnl2* expression was instead detected in samples of 48 hpf WT embryos. A significant reduction of the expression of all *metrn* genes could be measured using triplMut samples of the same age by qRT-PCR. These results suggest that the mRNA produced by the loci that we targeted is degraded by non-sense-mediated decay (Supplementary Fig. 1B). We performed *in situ* hybridization on *metrn* and *metrnl1* from 2-cells stage to 1-day post-fertilization (dpf) on triplMut embryos (Supplementary Fig. 1C) to confirm this hypothesis. No expression could be detected for neither of those two genes in the triplMut embryos, confirming the degradation of the transcripts in the *metrn* mutant backgrounds (Supplementary Fig. 1C).

Despite the absence of gross morphological defects, using *myl7* antisense riboprobe *in situ* hybridization in single mutant embryos, we observed a mis-positioning of the heart in triplMut mutant embryos. Indeed while 88.43% of the wild type control embryos had D-looped shaped hearts, only 38.17% of the triplMut embryos exhibited a WT-like heart looping phenotype (Table 1 and Fig. 1B-C). Similarly, *metrn*$^{-/-}$ and *metrnl1*$^{-/-}$ single mutant embryos displayed a higher proportion of randomized heart phenotypes (Table 1 and Fig. 1B-C). The injection of *metrn* and/or *metrnl1* mRNA into one-cell stage triplMut zebrafish embryos could partially rescue the observed phenotypes (Table 1, Supplementary Fig. 1D). In addition to the heart, morphological L–R asymmetry of the visceral organs was also perturbed in triplMut embryos (using *gata6* expression as a marker). Indeed, 10.49% of the triplMut embryos exhibited symmetrical placement of the gut and pancreas with respect to the midline and 9.88% heterotaxic phenotypes compared to the wild type embryos (WT: 93.84% L–R asymmetry, 4.79% L–R symmetry and 1.37% heterotaxia) (Fig. 1D-E). These results indicate that while

Metrns are not implicated in the specification of neither the heart nor the visceral organs (*myl7* and *gata6* expression being detected in triplMut embryos and in single mutants for *myl7*), their loss of function reveal that they are implicated in the L-R asymmetry positioning of these organs. The left-jogged and D-looped heart or the right-positioned liver are two of many examples of early L-R asymmetry determination in zebrafish and are well-studied readouts for altered L-R pattering processes. Therefore, our results suggest that Metrns might play a critical role in the establishment of L–R asymmetry during early development.

Metrns are required for proper Nodal factor genes expression

Nodal signaling is one of the major regulatory pathways for the determination of the L-R axis during vertebrate development. In zebrafish, null mutants for several Nodal factors like *spaw* (*Nodal* zebrafish orthologue), *dand5* or *lefty1* (*lft1*) all display symmetric or randomized heart looping and jogging similarly to *Nodal* mutant mice [25]–[28]. We therefore asked whether Metrns loss of function could affect the expression of these factors. To do so, we assessed *dand5*, *spaw*, *lft1* and *lft2* expression in our *metrns* mutant embryos. By qRT-PCR, we measured a significant reduction of *dand5* expression at 14 hpf in triplMut embryos compared to wild type controls (Fig. 2A). Similarly, the expression of *spaw*, *lft1* as well as *lft2* in the absence of Metrns proteins was also downregulated in triplMut embryos compared to wild type embryos (Fig. 2A).

We next characterized *dand5* specific R > L bias expression pattern in triplMut embryos by *in situ* hybridization. In more than 61% triplMut embryos, we could not detect *dand5* expression at 14 hpf and 23% displayed an abnormal *dand5* R > L expression bias (Fig. 2 B-C). In single *metrn*$^{-/-}$ and *metrnl1*$^{-/-}$ mutant embryos, *dand5* expression pattern was also altered (Supplementary Fig. 2A). These results are in line with previous findings reporting that *dand5* expression in the KV is only altered if upstream symmetry breaking mechanisms are disrupted [29]–[31]. We then also analyzed the gene expression patterns of *spaw*, *lft1* and *lft2* by *in situ* hybridization (Supplementary Fig. 2B). At 16 hpf *spaw* is normally expressed adjacent to the KV and in the left LPM. In *metrn*$^{-/-}$ and *metrnl1*$^{-/-}$ single mutants as well as triplMut embryos, we could not detect any *spaw* expression in the left LPM and only faintly around the KV (Supplementary Fig. 2B). The Spaw inhibitor *lft1* at this stage is expressed along the midline. In all analyzed *metrn* mutants (single *metrn* and *metrnl1* and triplMut), its expression was severely disrupted at the midline (Supplementary Fig. 2B, middle panel). The same was observed for *lft2* which expression in the left heart field was either absent or randomized in *metrn* mutants, single or triplMut embryos, compared to the wild type embryos (Supplementary Fig. 2B, lower panel). These results indicate that Metrns are required for the proper expression of Nodal factor genes that are determinants of proper L-R patterning.

Metrns are expressed during early zebrafish development

To investigate how Metrns affect the expression of Nodal factors during early development, we analyzed the pattern of expression of all three zebrafish *metrn* genes from 2 cell stage to 48 hpf. We first investigated the expression pattern of *metrn* and *metrnl1* by *in situ* hybridization and hybridization chain reaction (HCR) experiments. At the 2-cells stage, we detected both *metrn* and *metrnl1* maternally expressed transcripts (Fig. 3A, Supplementary. Fig. 3A). At 6 hpf (also called shield stage), *metrnl1* expression could be detected over the whole animal cap whereas zygotic *metrn* expression onset was observed only around the yolk syncytial layer (YSL) at this developmental stage (Fig. 3A). *Metrn* expression was then restricted to the developing LPM and to the leading edge of the shield from 9 hpf (Fig. 3A, Supplementary Fig. 3B). In comparison, *metrnl1* was found expressed throughout the whole enveloping layer and developing midline (Fig. 3A, Supplementary Fig. 3B). At 12 hpf, the expression of *metrn* was restricted to the KV area while *metrnl1* transcripts were mainly found in the midline (Fig. 3A-B). By HCR, we found both gene expression colocalizing in the area of the KV at 12 and 14 hpf (Fig. 3B). By 24 and 48 hpf, both genes were found strongly expressed in the central nervous system (CNS) (Supplementary Fig. 3C). Finally, *metrnl2* expression onset started from 24 hpf broadly in the embryonic brain (Supplementary Fig. 3C). At 48 hpf, *metrnl2* transcripts were mostly found in the otic vesicles and at the somite boundaries (Supplementary Fig. 3C).

We next analyzed the relative expression of *metrn* genes to landmarks of the KV structure like *casanova* (*cas*), a well-studied DFC marker [32], [33]. We observed a complete colocalization of *metrn*/*cas* and *metrnl1*/*cas* signals at 10 hpf, indicating that *metrns* genes are expressed in DFCs, the cells that will later form the KV (Fig. 3C-D). To assess whether *metrn* and *metrnl1* expression in the KV structure is conserved among vertebrates, we performed *in situ* hybridization for *metrn* and *metrnl1* in the chick embryo at early stages. Around stage HH6, we could observe *metrn* and *metrnl1* expression at the Hensen's node and around the primitive streak (marked by primitive streak landmark *fgf8*) (Supplementary Fig. 3D). Remarkably, the chick *metrn* and *metrnl1* expression patterns were reminiscent of the ones that we observed in zebrafish, suggesting that *metrn* genes expression at early developmental stages in the KV and midline structures is conserved throughout vertebrates.

Metrns loss-of-function leads to DFC disorganization and migration defects

The specific expression of *metrn* and *metrnl1* in DFCs and in the KV area at early developmental stages led us to ask what role they may play for these cells and the KV formation and function. Although *metrnl2* expression does not appear before 24 hpf, we used the triple mutant line triplMut that we generated throughout all subsequent analyses (if not

stated otherwise) due to possible genetic compensation effects that were reported in other studies [34]. To assess whether the loss of Metrn proteins function could affected the migratory and clustering properties of DFCs, we labeled these cells in 9 hpf (80-90% epiboly) gastrulating mutant embryos using the DFC landmarks *cas* [32], [33], *ntl* [35] or *sox17* [32]. Compared to wild type embryos displaying ovoid DFC clustering, about 65% of the triplMut embryos displayed multiple segregated DFC clusters or abnormal linear cellular distributions as shown using *cas* marker in 9 and 10 hpf triplMut embryos (Fig. 4A-B, Supplementary Fig. 4B). Similarly, *metrn*$^{-/-}$ as well as *metrnl1*$^{-/-}$ single mutant embryos presented clustering defects of *cas*-expressing DFC compared to wild type embryos (Fig. 4B, Supplementary Fig. 4A-B). In single or triplMut$^{+/-}$ heterozygous embryos, the DFC clustering was instead not significantly or very mildly affected as revealed (Supplementary Fig. 4B). The observed defects were also present when using *ntl* and *sox17* as DFC markers whose expression was detected at 8 and 10 hpf respectively, indicating that although disorganized, the DFCs identity was not altered by the absence of *metrns* expression (Supplementary Fig. 4C). Together, these results indicate that Metrns are required for the proper clustering of DFCs and subsequent KV formation.

It was reported that proper adherent cell assembly is crucial for DFCs directional collective cell migration during their animal to vegetal pole (AP to VP) journey [36] (Fig. 4C). We thereby evaluated the migration capacity of DFCs during early development of in the absence of Metrn proteins. To do so, we first labeled *cas*-expressing DFCs by *in situ* hybridization in wild type and triplMut embryos and measured the position of *cas*-expressing DFCs along the AP-VP axis divided by the total embryo length at 6 hpf, 8 hpf and 10 hpf. Compared to wild type embryos, DFCs in triplMut embryos showed migratory delays of about 8% to 13% at all analyzed developmental stages (Fig. 4D and Supplementary Fig. 4D). Together, our results indicate that DFCs migrate significantly slower in triplMut embryos compared to wild type DFCs, suggesting that Metrn proteins are important for both proper DFCs clustering and migration along the AP-VP axis.

***Metrns* loss-of-function impairs the KV formation and function**

At the end of gastrulation, DFCs that migrated to deeper layers of the developing zebrafish embryo form a lumen to shape the KV, a ciliated organ transiently present (from around 10.5 hpf to 30 hpf [37]) that is crucial for initiating L-R asymmetric patterning [9], [18]. As we observed at 14 hpf, it was reported that Dand5, a member of Cerberus/Dan family of secreted factors, is expressed adjacent to the KV with a right – left (R > L) bias between 11 and 14 hpf in zebrafish (Fig. 2) [38]. The right-biased expression of *dand5* was shown to be directly influenced by the direction and the strength of the Nodal flow generated by the KV [39]. In return, Dand5 contributes to the left-biased expression of *spaw* in the LPM by antagonizing

Spaw activity [38]. The leftward-directed flow generated by the KV was also shown to be important for the asymmetric expression of other Nodal genes, like *spaw*, *lefty1* (*lft1*) and *lefty2* (*lft2*) [19], [20]. The observed disturbed expression of these Nodal factors in the absence of Metrns led us to hypothesize that Metrn proteins might not only be critical for the proper clustering and migration of DFCs but also for the proper formation and function of the KV. To assess this question, we first labeled the cilia present in the KV of wild type and triplMut embryos at 14 hpf with α-AT (Fig. 5A). We then measured the KV diameter and compared the number of cilia present in the KV of both wild type and triplMut embryos at this developmental stage (Fig. 5B-C). Compared to wild type control embryos, the KV diameter and the number of KV cilia were significantly reduced in the triplMut embryos (Fig. 5B-C). Previous work has shown that these two parameters present high variability from one embryo to the other, contrary to the overall KV cilia length [40]. Compared to the wild type controls, triplMut embryos also displayed a significant reduction in the KV cilia length (Fig. 5D). These results indicate that the loss of Metrns function also impacts the proper KV formation.

We next evaluated whether the reduced number and length of cilia in triplMut altered KV function. To do so, we compared the Nodal flow generated by the KV of triplMut embryos to the one of wild type embryos. The movement generated by the KV cilia was monitored by injecting fluorescent microspheres (0.5µm) into the KV at 12-14 hpf. To quantify the flow inside the KV, fluorescent microbeads movement was tracked in wild type control (n = 363 beads in 4 embryos) and in triplMut embryos (n = 318 beads in 4 embryos) (Fig. 5E). Beads movement analysis within the KV showed a counter-clockwise rotation of the flow in wild type control (Fig. 5E, Supplementary Movie 1). In contrast, this movement was severely impaired in triplMut embryos (Fig. 5E, Supplementary Movie 2). To quantify the properties of the beads displacement, we computed the mean square displacement (MSD), which enables to distinguish between directed and confined motion. This analysis revealed a directed motion of the microbeads in the wild type KV (MSD quadratic dependence on Δt) and a confined motion (MSD asymptotic behavior) in triplMut [41]. Accordingly, measurement of average bead velocity showed an overall reduction in the beads speed in the triplMut mutant embryos compared to the wild type controls (Supplementary Fig. 5). These results demonstrate that the observed defects in the KV formation in the absence of Metrns also severely impacts its function and thereby the flow generation, responsible for the proper Nodal factors expression.

Genetic interaction of ItgαV/Itgβ1b and Metrns on the level of the DFCs

In order to uncover one of the mechanisms through which Metrn proteins act in the establishment of the early L-R patterning, we finally assessed the possible relationship between Metrns and mediators of the extracellular matrix like Integrin αV1 (ItgαV1) and

Integrin β1b (Itgβ1b) at the level of DFCs, in particular for their proper clustering and migration. Integrins are membrane receptors involved in cell adhesion and recognition notably during embryogenesis [42]. During gastrulation, *itgαV* as well as *itgβ1b* were shown to be expressed in DFCs and *itgαV* and *itgβ1b* morpholino-injected embryos display DFC phenotypic defects reminiscent to those observed in *metrn* mutants [43]. In order to test whether ItgaV1 and Itgβ1b and Metrns genetically interact, we injected insufficient doses of morpholinos for *itgβ1b* (0.5 ng) or *itgαV1* (0.41ng) into 1 to 4 -cell stage in a heterozygous *metrns* mutant background. The injection of the morpholinos at these doses and at sufficient doses (*itgβ1b:* 0.7ng, *itgαV1:* 1.25ng) reproduced the previously reported defects on DFCs (Fig. 6A, Table 2) [43]. Instead, the injection of low doses of either *itgβ1b* or *itgαV1* morpholino did not affect DFC clustering, similarly to non-injected triplMut$^{+/-}$ embryos (Fig. 6A, Table 2). However, a significantly higher percentage of embryos with DFC clustering defects could be observed upon the injection of either morpholino at low dose into triplMut$^{+/-}$ (Fig. 6A, Table 2). These results are consistent with the hypothesis that Metrn proteins act together with both Integrins for the proper clustering and migration of DFCs during early embryonic development.

DISCUSSION

Our results demonstrate a novel role for Meteorin proteins during vertebrate embryonic development. We showed that Metrns are required for symmetry breaking and the establishment of L-R asymmetry. We demonstrate that Metrns ensure this function by acting together with Integrins ItgαV1 and Itgβ1b for the proper clustering and migration of DFCs to form the KV. We could show that Metrns are essential for several aspects of the KV formation and function like the cilia length, cilia number, KV size and expression of Nodal flow genes and that the regulation of all these parameters by Metrn proteins is critical for the proper asymmetric positioning and morphology of vital organs like the heart (Fig. 6B).

From 9 hpf the expression of *metrn* was visible around the developing LPM close to the midline and the leading edge of the shield. *Metrnl1* expression was found throughout the whole enveloping layer and the developing midline which plays an important role in vertebrate L-R development. Zebrafish midline mutants display altered *lft1* and *lft2* expression patterns as well as discordance among heart, gut and brain gene expression patterns [44]. However, we hypothesize that the described body asymmetry defects in our Metrn mutants probably do not originate from impaired midline structures but rather impaired DFC clustering and migration. TriplMut$^{-/-}$ embryos indeed had intact *ntl*-positive notochords (Supplementary Fig. 4C), as well as randomized visceral organs positioning (Fig. 1D-E), phenotypes that are not characteristic for defects of the anterior midline [44].

DFCs are precursors of the zebrafish KV, organ of laterality, essential for the L-R axis establishment. DFCs develop at the beginning of gastrulation and form the KV by the end of gastrulation [9], [18]. Given the early onset of *metrn* and *metrnl1* expression and their specific expression within the DFCs we investigated their role for the clustering and migration capacity of DFCs during these early embryonic developmental steps. In the course of their migration, DFC progenitors intercalate mediolaterally and results in an oval-rosette shape cluster of DFCs by mid-gastrulation that will form the KV [17]. *Metrn$^{-/-}$, metrnl1$^{-/-}$* and triplMut zebrafish embryos displayed DFC assembly defects and delayed migration of these cells during gastrulation. Since DFCs in triplMut still express DFC specific markers (*sox17, cas, ntl*), we concluded that Metrns are not required for the specification of DFCs *per se* but rather that Metrns are solely important for their proper clustering and migration.

It is important to note that the DFC clustering and migration defects observed in Metrn mutants does not only appear to be affected along the mediolateral axis but also apico-ventrally since the connection between DFCs and the YSL/EVL seems also disrupted in these mutants (Fig. 4A). It is therefore possible that the observed defects are due to impaired embedding of the DFCs into the cells of the EVL, the deep cell layer and the EVL. Since the proper connection between DFC and EVL enables a subset of DFCs to have apical contacts with the EVL and to

be pre-polarized, one can speculate that Metrns play a role in the polarization and direct apical contacts establishment of DFCs to the EVL [17], [18], [45], [46]. We hypothesize that the observed clustering defects in *metrn* mutants might instead be due to a role of Metrns in DFC-DFC contact interaction [44]. Additionally it was shown that the formation of the developing KV lumen was directly connected to ciliogenesis as polarized DFCs initiated developing cilia at their membrane domain facing the forming lumen [17]. This indicates that proper DFC polarization is essential for the KV formation and for ciliogenesis. The decreased number of cilia in *metrn* mutants indicate a lower number of DFCs giving rise to the KV in these mutants and the reduced cilia length highlights an impairment of their polarization consequently leading to KV formation and function defects.

In line with the impaired KV formation and function in *metrns* mutants, it was shown that knockdown of Integrin αV as well as Integrin β1b in zebrafish results in L-R asymmetry defects [43]. This was explained by DFC organization and migration defects and disturbed KV formation. Integrin αVβ1 specific functions have not yet been completely resolved in mammals, mostly due to their broad expression and redundant function with other integrins as well as the lack of antibodies and inhibitors specific for αVβ1. However, several *in vitro* studies already connected αVβ1 to developmental processes. For instance, αVβ1 was shown to be implicated in embryonic astrocytes and oligodendrocyte precursors migration in rodents [47] and neural cell adhesion molecule L1 cell binding [48]. Our results suggest that Integrin αV/β1b genetically interacts with Metrn proteins as one mechanism to properly cluster DFCs. Their interaction could influence Integrin's adhesive functions (or other properties) necessary for DFC clustering. Consequently, the absence of Meteorins would possibly leads to disturbed adhesion and/or Integrin signaling, resulting in DFC assembly defects and disturbed KV development, as discovered in *metrn* mutants.

Despite the recent advancements in uncovering the multiple functions of Meteorins, their receptors during early development are still unknown. It was recently shown that METRNL is promoting heart repair through its binding to the KIT tyrosine kinase receptor, establishing METRNL as a KIT receptor ligand in the context of ischemic tissue repair [49]. In another study, it was reported that Metrn is a ligand for the 5-hydroxytryptamine receptor 2b (Htr2b). Additionally Metrn was associated to regulating reactive oxygen species levels in hematopoietic stem/progenitor cells via directing phospholipase C signaling [50]. Analyzing the expression of *kita* at 9 hpf (one of the zebrafish KIT tyrosine kinase receptor paralogs), we found that *kita* is solely expressed in the prechordal plate and from 11 hpf in the lateral borders of the anterior neural plate (Supplementary Fig. 6A). Its paralog *kitb* is expressed from 11 hpf

in the anterior ventral mesoderm (Supplementary. Fig. 6B), as previously reported [51]. Analyzing then *htr2b* expression during zebrafish development, we found it only expressed from around 2 dpf in the heart (Supplementary. Fig. 6B). Thus, the absence of *kita/b* as well as *htr2b* expression at early embryonic stages in proximity of the DFCs and in the forming KV suggests that Metrns rather act through other receptor(s) to ensure their L-R patterning functions.

Mechanisms underlying L-R patterning are known to be highly conserved within vertebrates. Hence, we raised the question whether Meteorin protein family is conserved across different species. Genes coding for *metrn* and *metrnl* are existing in several vertebrates classes, but could not be found in genomes of invertebrates [52]. *Metrnl* paralogues genes could instead be found in amphioxus and tunicates. Therefore, we suggest that Metrn proteins arose after the Chordate evolution and their function in the establishment of the L-R axis is specific for Chordates (Supplementary Fig. 6C).

MATERIAL AND METHODS

Zebrafish husbandry

Zebrafish (Danio rerio) were maintained at 28°C overnight (O/N) a 14 hours light/10 hours dark cycle. Fish were housed in the animal facility of our laboratory which was built according to the respective local animal welfare standards. All animal procedures were performed in accordance with French and European Union animal welfare guidelines with protocols approved by the committee on ethics of animal experimentation of Sorbonne Université (APAFIS#21323- 2019062416186982).

Metrn, *metrnl1* and *metrnl2* CRISPR-Cas9-mediated mutagenesis

SgRNA guide sequences were cloned into a BsaI-digested DR274 plasmid vector (Addgene 42250). The sgRNAs were synthetized by *in vitro* transcription using (using the Megascript T7 transcription kit, Ambion, AM1334). After transcription, sgRNAs were purified using a RNAeasy Mini Kit (Qiagen). The quality of purified sgRNAs was checked by electrophoresis on a 2 % agarose gel. The target sequences were the following:

	Sequence (5'->3')
metrn	CCACCACACCCGGCCCAGCC
metrnl1	GGTGTATCTCCGCTGCGCCC
metrnl2	CCAGAAACAGCGCCCCCTCC

Cas9 mRNA was generated as described in Hwang, Fu et al. 2013 [53]. To induce targeted mutagenesis at the *metrn, metrnl1* and *metrnl2* loci, 200 ng/ml of sgRNA were injected into one-cell stage zebrafish embryos together with 150 ng/ml of *cas9* mRNA. Injected embryos were grown to adulthood and screened for mutation in their offspring.

DNA extraction and sequencing for analysis of CRISPR/Ca9- mediated mutagenesis

For genomic DNA extraction, pools of 5 dpf embryos were digested for 1 h at 55 °C in 0.5 mL lysis buffer (10 mM Tris, pH 8.0, 10 mM NaCl, 10 mM EDTA, and 2% SDS) with proteinase K (0.17 mg/mL, Roche Diagnostics) and inactivated 10 min at 95 °C. To check for frequency of indel mutations, target genomic loci were PCR amplified using a Phusion High-Fidelity DNA polymerase (Invitrogen). PCR amplicons were subsequently cloned into a pCR-bluntII-TOPO vector (Thermo Fisher). Plasmid DNA was isolated from single colonies and Sanger sequencing was performed by Eurofins. Mutant alleles were identified by comparison with the wild type sequence using Geneious software.

Mutants genotyping and generation of triple mutants

Genotyping of *metrns* mutants was performed as follows: after genomic DNA extraction PCR amplification reactions were conducted in final volumes of 20 µl containing 1x PCR reaction buffer, 1,5mM MgCl2, 70 ng of gDNA, Taq DNA Polymerase (5U/µl) and 0.5 µM of each primer.

	Sequence (5'->3')
***metrn*-fw**	CTGTGTTGACTGCTGGCTG
***metrn*-rv**	GTGGTTTAGTGGTGTTCTTACAATGA
***metrnl1*-fw**	TCCCATGCCTGGACCTCATA
***metrnl1*-rv**	AGACGGAGAGAAGAGACGCT
***metrnl2*-fw**	TGTTGATCAGCAGTGTGTGCGTAGC
***metrnl2*-rv**	GTCCTCCGCTGATCTACGTG

The DNA amplification was performed with 35 cycles at the annealing temperature of 60°C. *Metrn* and *metrnl2* amplicons were loaded on 2 % agarose gel to discriminate between wild type and mutant alleles (for *metrn*, the expected size of wild type amplicon is 598 bp while the mutant amplicon is 482 bp long using the same primer set; for *metrnl2*, the size of the expected wild type amplicon is 242 bp while the mutant band is 156 bp long using the same primer set). *Metrnl1* PCR product was digested at 55°C O/N with the PasI restriction enzyme and the resulting digestion was subsequently analyzed on a 2% agarose gel. The wild type amplicon results in two fragments of 107 bp and 94 bp length, respectively. The mutant amplicon band size is instead 201 bp using the same primer set. Triple mutants were obtained by incrossing homozygous *metrn* and *metrnl1* mutants to generate double heterozygous mutants. Double heterozygous mutants were then crossed with homozygous *metrnl2*$^{-/-}$ fish and genotyped to identify triplMut$^{+/-}$ triple heterozygous mutants. triplMut$^{+/-}$ fish were incrossed and genotyped to identify triplMut$^{-/-}$ triple homozygous mutants. In all described experiments of this study, triplMut$^{+/-}$ were obtained by outcrossing female triplMut$^{-/-}$ fish with male wild type fish, if not stated differently to prevent from *metrns* maternal contribution.

Hybridization chain reaction (HCR)

All HCR probes and solutions were purchased from Molecular Instruments®. Dechorionated embryos at the developmental stage(s) of interest were fixed in 4% paraformaldehyde in PBS (pH 7.4) for 2 hours at room temperature, followed by several washes with PBS to stop the fixation. Embryos were then dehydrated with a series of methanol (MeOH) washes and stored at -20 °C. The HCR was performed following the manufacturer's instructions. HCR samples were imaged on an inverted confocal microscope Olympus FV-1000, employing a 20x oil

immersion objective (NA 0.85). Z-volumes were acquired with a 5 µm resolution and images were processed and analyzed using ImageJ.

In situ hybridization in zebrafish and chicken

The respective cDNA fragments were amplified by PCR from total zebrafish or chicken cDNA of stage 12 hpf – 48 hpf and HH6. *In vitro* transcription of Digoxigenin/Fluorescent-labeled probes was performed using an RNA Labeling Kit (Roche Diagnostics Corporation) according to manufacturer's instructions. Zebrafish and chicken whole-mount *in situ* hybridizations was performed as previously described [54] [55]. Stained embryos were then imaged on a Leica MZ10F stereomicroscope. Images were processed and analyzed using ImageJ software. Color balance, brightness and contrast and were applied uniformly. Fluorescently-labeled samples were imaged using an inverted confocal microscope Olympus FV-1000, employing a 40x oil immersion objective (NA 1.30). Z-volumes were acquired with a 0.5 µm resolution and images were processed and analyzed using ImageJ.

Analysis of DFC phenotype and migration

For the DCF clustering analysis, Bayesian inference was used to recover the maximum-likelihood value for the malformation probability. The outcome of an experiment was considered to be a binary random variable (malformed or wild type phenotype) whose probability depends solely on the experimental condition. The total number of malformed phenotypes per experiment is therefore binomially distributed. The posterior distribution is obtained by inverting this binomial distribution using Bayes theorem, under a uniform prior. Under these hypotheses the maximum-likelihood estimate for the malformation probability is simply given by the empirical malformation frequency. The standard deviation of the posterior distribution was used to provide a confidence interval for the estimate (black error bars). *P*-values were evaluated using Fisher exact test on the number of malformed and wild type phenotypes. AP to VP DFC migration was calculated as the percentage of the total embryo length.

qRT-PCR and analysis

For gene expression analysis total RNA extraction was prepared from zebrafish embryos with TRIzol reagent (Thermo Fisher) and TURBO DNA-free reagents (Invitrogen™ AM1907M). Total RNA was cleaned up using RNeasy Mini Kit (Qiagen) following the manufacturer's instructions and treated twice with DNase I (1 U/µg RNA, Qiagen). The RNA concentration was quantified using the Nanodrop2000 (Thermo Fisher). RNA (1 µg) was retrotranscribed using random primers and a SuperScript III First-Strand Synthesis system (Invitrogen 18080051). For qRT-PCR, the SYBR Green PCR Master Mix (Thermo Fisher) was used

according to the manufacturers protocol. *Ef1a* was used as reference genes as previously reported [56]. All assays were performed in triplicates and repeated in 3 independent experiments. The mean values of triplicate experiments were calculated according to the delta CT quantification method [57] and a student T-test was applied for the *p*-value calculation.

mRNA synthesis and injection

Zebrafish *metrn* and *metrnl1* cDNA fragments were amplified by PCR from zebrafish cDNA of 1 dpf. The fragments were cloned into a *pCS2+* plasmid linearized with Xho1 and Xba1 restriction enzymes using a Quick Ligation Kit (NEB). Each plasmid was then linearized with NotI restriction enzyme and mRNAs were synthesized by *in vitro* transcription (using the mMESSAGE mMACHINE sp6 Ultra kit AM1340, Ambion) adding 1 µL of GTP (provided in the kit) and followed by lithium chloride precipitation. 150 ng/µl of the synthesized mRNAs were then injected into 1- to 4-cell-stage zebrafish embryos.

Design and injection of antisense morpholino oligonucleotides

The published morpholinos (MO) used in this study for *itgαV* (5'-AGTGTTTGCCCATGTTTTGAGTCTC-3'), *itgβ1b1* (5'-GGAGCAGCCTTACGTCCATCTT AAC-3') and for control (ctrl MO) (5'-CCTCTTACCTCAGTTACAATTTATA-3') were injected using the same reported concentration of 0.41 ng (*itgαV*) and 0.5 ng (*itgβ1b1*) for insufficient doses, 1.25 ng (*itgαV*) and 0.7 ng (*itgβ1b1*) for full knock down effect and 2.5 ng for the ctrl MO [43]. All MOs were obtained from Gene Tools (Philomath, OR, USA). MOs were injected in 1- to 4- cell-stage zebrafish embryos.

Whole-mount immunohistochemistry and quantification

Embryos were fixed in 4% paraformaldehyde in PBS-Tween for 2h at room temperature (RT) and subsequently washed three times in PBS-1% Triton X-100 to promote their permeabilization. Consequently, they were incubated for 1 hour at RT in blocking solution (10% Normal Goat Serum, in PBS-Tween) followed by overnight incubation, at 4 °C, with a 1/200 dilution of a mouse anti- acetylated tubulin monoclonal antibody (Sigma T6793) in blocking solution. After five washes in 1x PBS-Tween, the embryos were incubated O/N with an Alexa Fluor 488 anti-mouse IgG secondary antibody (Life Technologies, A28175) diluted at a final concentration of 1/200 respectively in 1% blocking solution. The following day embryos were washed five times in 1x PBS-Tween and mounted in 1% low-melting point agarose in glass-bottom cell tissue culture dish (Fluorodish, World Precision Instruments, USA).

An inverted confocal microscope Olympus FV-1000 was used for imaging, employing a 40x oil immersion objective (NA 1.30). Z-volumes were acquired with a 0.5 µm resolution and images were processed and analyzed using ImageJ.

Fluorescent microspheres injection and analysis

FluoSpheresH fluorescent microspheres injection was conducted as previously described [58]. Embryos were embedded in 1% low melting-point agarose diluted in egg water. Imaging was performed with a 40x water dipping objective using an upright Yokogawa CSU-X1 spinning disk scan head, mounted on a DM6000 upright Leica microscope and a CCD CoolSnap HQ2 camera at 4 Hz using the green channel at 0.25 µm resolution on a single Z-plane. Beads trajectory tracking was performed using an already developed toolbox [59]. The size detection parameter was set to 0.75 – 1.25 µm objects with a brightness superior to the 0.01 percentile of the whole image. Objects that travelled less than 2.5 µm between two consecutive frames were linked into the same trajectory. Analyses were then performed using a custom-made Matlab code. For better visualization, trajectory plots only show 20 tracked beads. MSD analysis was conducted using an already published code (https://tinevez.github.io/msdanalyzer/) [60]. Average mean square displacement (MSD) plots only show particle tracked between 1 and 8 seconds. Very short tracking durations do not permit to correctly estimate displacement properties and less then 1% of the particles were tracked for more than 8 seconds.

Phylogenetic analysis

Protein sequences were obtained from the Ensembl Genome Browser or UniProt. The following sequences were used: *D. rerio* Metrn (ENSDARP00000041804.5), *D. rerio* Metrnl1 (ENSDARP00000131064.1), *D. rerio* Metrnl2 (ENSDARP00000126894.1), *G. gallus* Metrn (ENSGALP00010026416.1), *G. gallus* Metrnl (ENSGALP00010044844.1), *H. sapiens* METRN (ENSP00000455068.1), *H. sapiens* METRNL (ENSP00000315731.6), *M. musculus* METRN (ENSMUSP00000127275.2), *M. musculus* METRNL (ENSMUSP00000038126.8), *X. leavis* Metrnl (ENSXETP00000107425.1), *L. oculatus* Metrn (ENSLOCP00000003703.1), *L. oculatus* Metrnl (ENSLOCP00000017224.1), *B. lanceolatum* (A0A8K0F3K3), *S. clava* (XP_039261436). *L. oculatus* was choosen as outgroup, *B. lanceolatum* as an example for Cephalochordata and *S. clava* as a representative for Tunicata. The phylogenetic tree was reconstructed with the phylogeny analysis from www. phylogenie.fr [61]–[67].

FIGURES

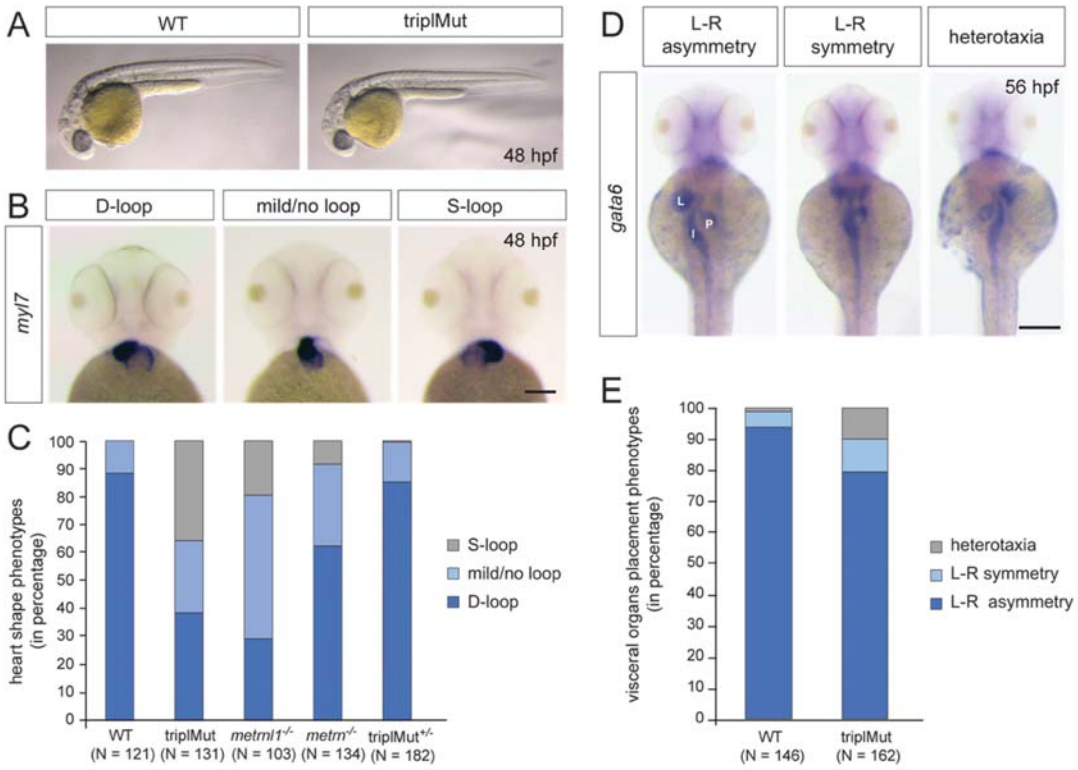

Fig. 1. Metrns loss-of-function causes heart jogging/looping and visceral organs -positioning defects. (**A**) 48 hpf triplMut zebrafish display no gross phenotypic defects compared to wild type (WT) embryos. (**B**) Examples of 48 hpf embryos showing mRNA expression of the heart marker *myl7* and the different heart looping phenotypes (ventral view). (**C**) Quantification in percentage of heart looping phenotypes at 48 hpf in WT, triplMut, *metrn*$^{-/-}$, *metrnl1*$^{-/-}$, triplMut$^{+/-}$ embryos. (**D**) Example of 56 hpf embryos showing *gata6* mRNA expression highlighting the different visceral organ positioning phenotypes (ventral view). (**E**) Quantification in percentage of visceral organ positioning phenotypes at 56 hpf in WT and triplMut embryos. In (D) L = liver, P = pancreas, I = intestine. Scalebars in (**B**): 100 µm, (**D**): 500 µm..

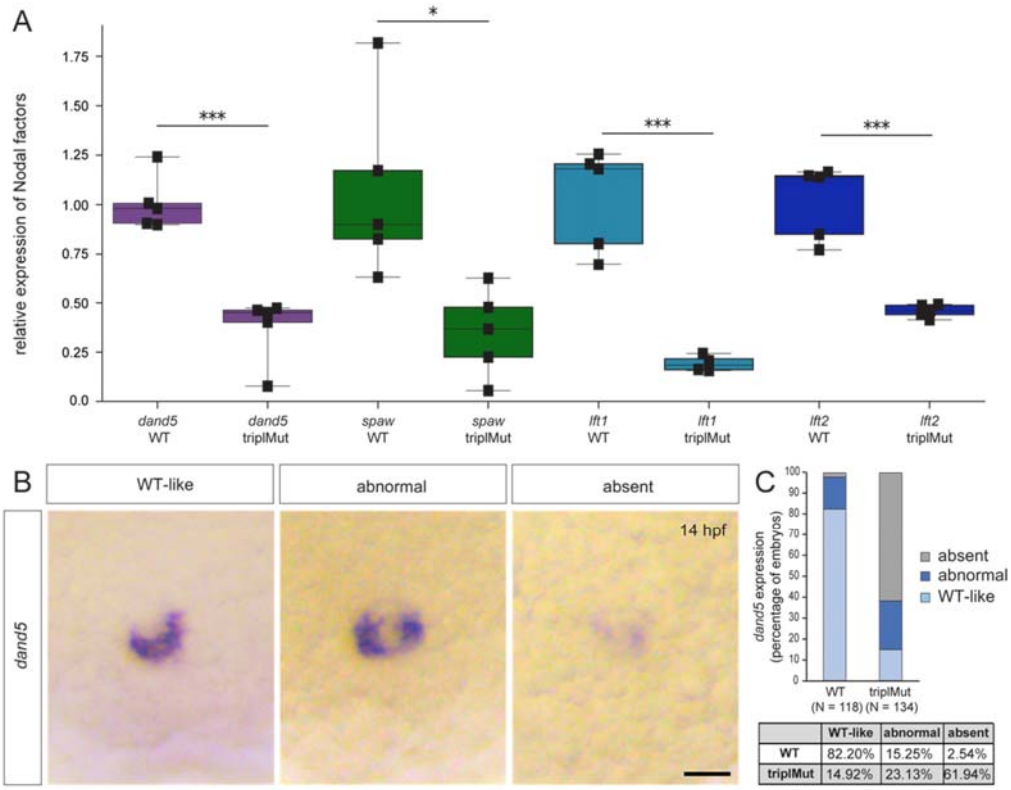

	WT-like	abnormal	absent
WT	82.20%	15.25%	2.54%
triplMut	14.92%	23.13%	61.94%

Fig. 2. Metrns are required for proper Nodal factor genes expression. (**A**) qRT-PCR analysis for *dand5*, *spaw, lft1* and *lft2* expression in 14 hpf wild type (WT) and triplMut embryos (Student t-tests, ****p*-value: 0.00019 for *dand5*, **p*-value: 0.014 for *spaw*; ****p*-value: 0.0004 for *lft1*; ****p*-value: 0.00019 for *lft2*). (**B**) *Dand5* expression at 14 hpf as revealed by *in situ* hybridization showing different transcripts distribution of *dand5* mRNA. (**C**) Quantification in percentage of *dand5* expression phenotypes at 14 hpf in WT and triplMut embryos. Scalebar in (**B**): 100 µm.

553

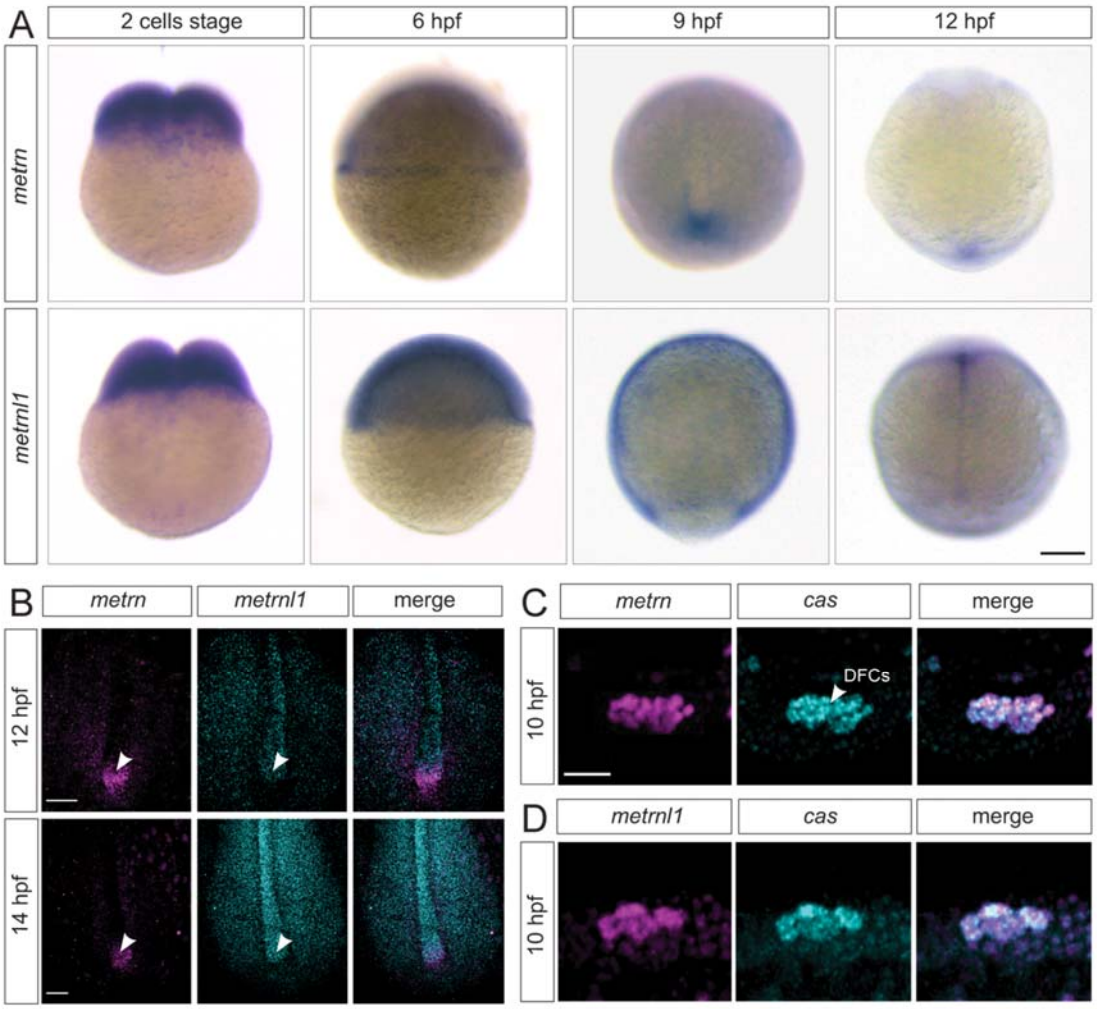

Fig. 3. *Metrns* are expressed during early zebrafish development. (**A**) Expression patterns of *metrn* and *metrnl1* during early embryonic development from 2-cell stage to 12 hpf. (**B**) Confocal cross-section of the midline region of 12 and 14 hpf zebrafish embryo showing mRNA expression of the *metrn* (magenta) and *metrnl1* (cyan) and their co-expression in the area of the Kupffer's vesicle (KV, indicated by arrow heads) (merge) by HCR. (**C**) *Metrn* and *cas* are co-expressed by dorsal forerunner cells (DFCs) as shown by double fluorescence *in situ* hybridization against *metrn* (magenta) and *cas* (cyan) on 10 hpf wild type embryos. (**D**) *Metrnl1* and *cas* are co-expressed by DFCs as shown by double fluorescence *in situ* hybridization against *metrnl1* (magenta) and *cas* (cyan) on 10 hpf wild type embryos. Scalebars in (**A**): 500 μm, (**B**) 250 μm, (**C**) and (**D**): 50 μm.

554

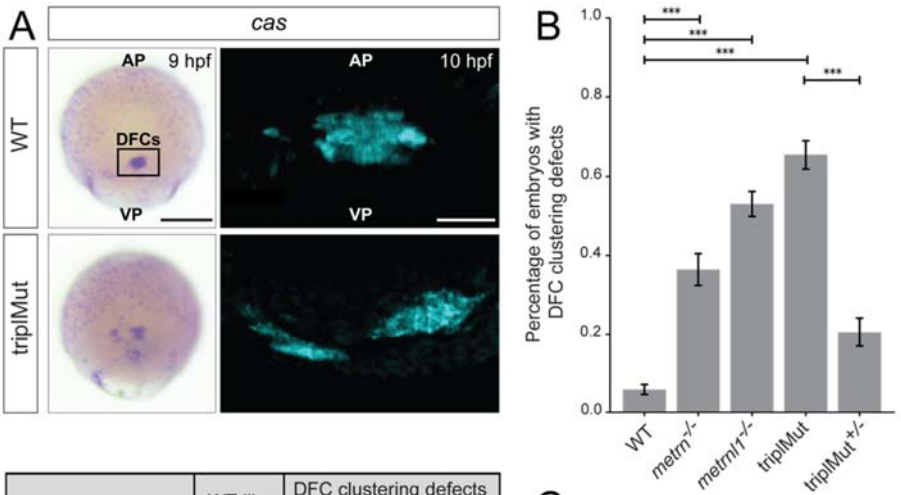

	WT-like	DFC clustering defects (% of embryos)
WT (N = 202)	93.07%	6.93%
metrn$^{-/-}$ (N = 140)	63.57%	36.43%
metrnl1$^{-/-}$ (N = 245)	46.94%	53.06%
triplMut (N = 182)	34.62%	65.38%
triplMut$^{+/-}$ (N = 140)	79.51%	20.49%

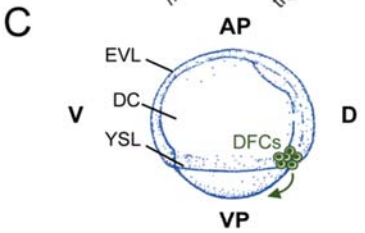

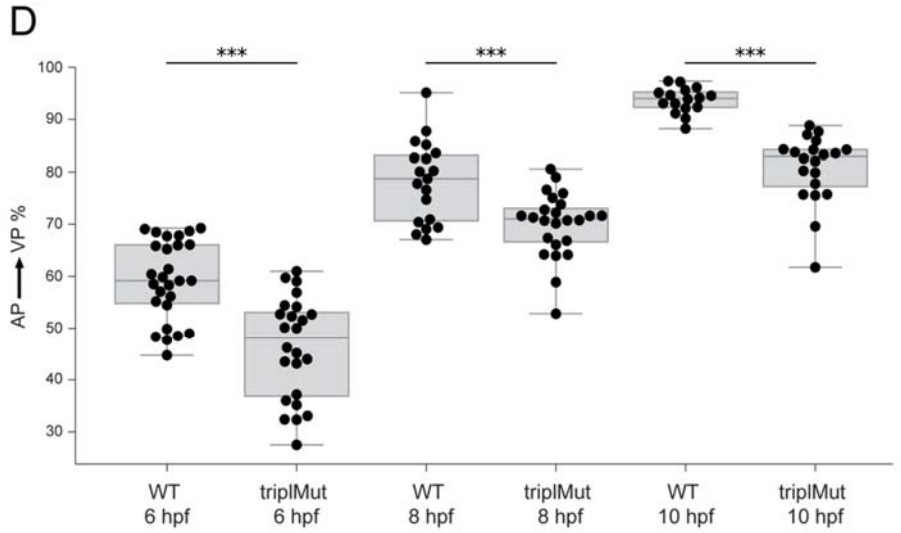

	6 hpf	8 hpf	10 hpf
WT	59.32% (+/- 7.65%, N = 27)	78.18% (+/- 7.94%, N = 19)	93.67% (+/- 2.48%, N = 16)
triplMut	46.26% (+/- 9.83%, N = 24)	69.94% (+/- 6.22%, N = 24)	80.67% (+/- 6.56%, N = 20)

Fig. 4. *Metrns* loss-of-function leads to DFC clustering and migration defects. (**A**) *Cas* expression in DFCs at 9 hpf and 10 hpf (cyan) in wild type (WT) and triplMut embryos reveals DFC misclustering in triplMut embryos. (**B**) Quantification in percentage of embryos with DFC clustering defects at 9 hpf in WT, *metrn*$^{-/-}$, *metrnl1*$^{-/-}$, triplMut and and triplMut$^{+/-}$ embryos (Fisher exact test, ****p*-value: 1.6e-07 for WT vs. *metrn*$^{-/-}$; ****p*-value: 3.5e-40 for WT vs. *metrnl1*$^{-/-}$; ****p*-value: 1.5e-49 for WT vs. triplMut and ****p*-value: 7.9e-15 for triplMut vs. triplMut$^{+/-}$). (**C**) Lateral view of a schematic

representation of an 8 hpf zebrafish embryo visualizing animal pole (AP) to vegetal pole (VP) dorsal forerunner cell (DFC) migration from both poles, adapted from [37]. EVL, enveloping layer; DC, deep cells; YSL, yolk syncytial layer; D, dorsal; V, ventral. (**D**) DFC migration quantification calculated as the percentage of the total embryo length at 6, 8 and 10 hpf in WT vs. triplMut embryos. Per condition and group 16 to 27 embryos were analyzed (Fisher exact test, ***p-value: 2.5e-06 for 6 hpf, ***p-value: 0.00038 for 8 hpf and ***p-value: 1.1e-08 for 10 hpf). Scalebars in (**A**, 9 hpf): 250 µm, (**A**, 10 hpf): 500 µm.

555

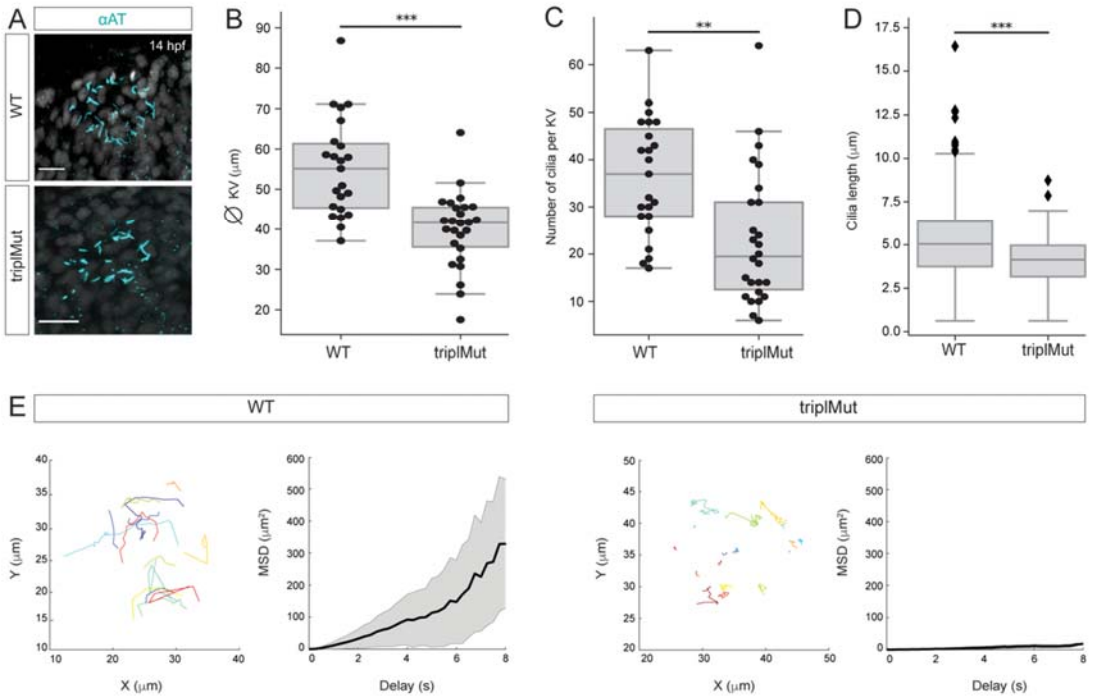

Fig. 5. *Metrns* loss-of-function impairs the Kupffer's vesicle formation and function. (**A**) Confocal cross-section of 14 hpf wild type (WT) and triplMut counterstained with acetylated tubulin (α-AT) labeling the cilia of the Kupffer's vesicle (KV). (**B**) The KV diameter size measurement, (**C**) cilia number per KV quantification and (**D**) individual cilia length measurement in WT and triplMut embryos at 14 hpf are all significantly decreased in triplMut (Student t-tests, ***p-value: 9.7e-06 for KV diameter size, **p-value: 0.0012 for cilia number and ***p-value: 1.2e-20cilia length). (**E**) Single microbeads tracking in the KV of 12 hpf -14 hpf WT and triplMut embryos and the mean square displacement (MSD), revealing a directed trajectory in WT samples in contrast to triplMut, displaying short and undirected trajectories**.** Scalebar in (**A**): 20 µm.

556

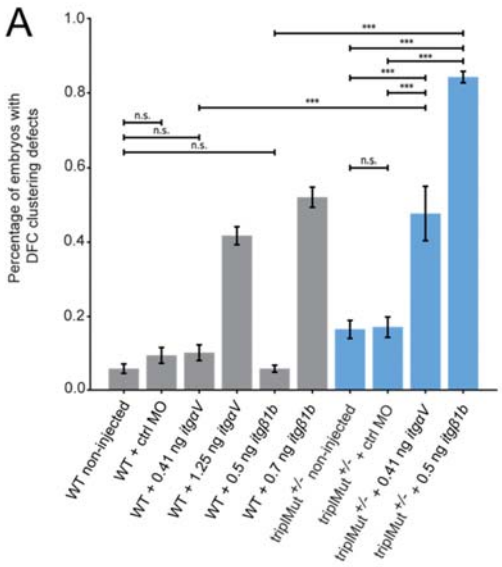

	WT-like	DFC clustering defects
WT non-injected	94.22%	5.78%
WT + ctrl MO	90.62%	9.38%
WT + 0.41 ng *itgαV*	89.90%	10.10%
WT + 1.25 ng *itgαV*	58.25%	41.75%
WT + 0.5 ng *itgβ1b*	94.22%	5.78%
WT + 0.7 ng *itgβ1b*	47.92%	52.08%
triplMut$^{+/-}$ non-injected	83.56%	16.44%
triplMut$^{+/-}$ + ctrl MO	82.95%	17.05%
triplMut$^{+/-}$ + 0.41 ng *itgαV*	35.16%	64.84%
triplMut$^{+/-}$ + 0.5 ng *itgβ1b*	15.74%	84.26%

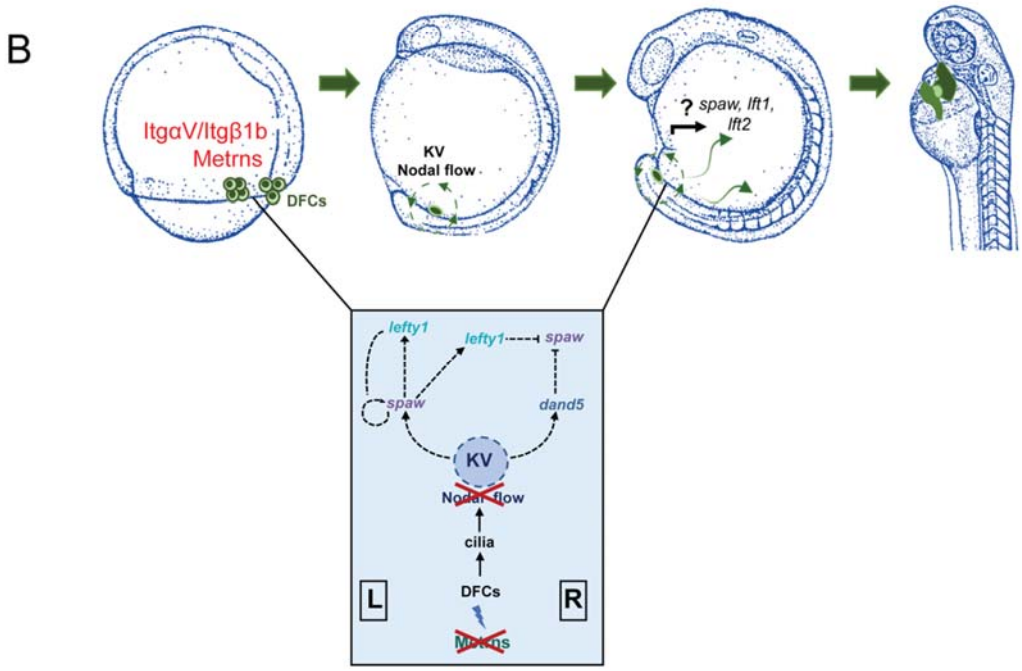

Fig. 6. Metrns and ItgαV/Itgβ1b act together for the proper clustering and migration of DFCs. (**A**) Quantification in percentage of embryos with DFC clustering defects at 9 hpf in non-injected wild type (WT), WT + 2.5 ng control morpholino (WT + ctrl MO), WT + insufficient doses of *itgαV/itgβ1b* MOs (WT + 0.41 ng *itgαV*; WT + 0.5 ng *itgβ1b*), WT + sufficient *itgαV/itgβ1b* MO doses (WT+ 1.25 ng *itgαV*; WT + 0.7 ng *itgβ1b*), triplMut$^{+/-}$ non-injected, triplMut$^{+/-}$ + 2.5ng ctrl MO and triplMut$^{+/-}$ with insufficient doses of *itgαV/itgβ1b* MOs (triplMut$^{+/-}$ + 0.41 ng *itgαV*; triplMut$^{+/-}$ + 0.5 ng *itgβ1b*). Fisher exact tests indicate **p*-value < 0.01, ***p*-value < 0.001 and ****p*-value < 0.0001 and ns = not significant. (**B**) Schematic representation modeling the novel role of Metrns for DFCs assembly and

migration, for the proper KV formation and subsequent Nodal factors expression distribution at the base of the correct L-R axis establishment during early development (adapted from [37]).

REFERENCES

[1] M. Blum, K. Feistel, T. Thumberger, and A. Schweickert, “The evolution and conservation of left-right patterning mechanisms,” *Development*, vol. 141, no. 8, pp. 1603–1613, Apr. 2014, doi: 10.1242/dev.100560.

[2] M. Blum and T. Ott, “Animal left–right asymmetry,” *Current Biology*, vol. 28, no. 7, pp. R301–R304, Apr. 2018, doi: 10.1016/j.cub.2018.02.073.

[3] D. T. Grimes and R. D. Burdine, “Left–Right Patterning: Breaking Symmetry to Asymmetric Morphogenesis,” *Trends in Genetics*, vol. 33, no. 9, pp. 616–628, Sep. 2017, doi: 10.1016/j.tig.2017.06.004.

[4] A. Kawasumi *et al.*, “Left–right asymmetry in the level of active Nodal protein produced in the node is translated into left–right asymmetry in the lateral plate of mouse embryos,” *Developmental Biology*, vol. 353, no. 2, pp. 321–330, May 2011, doi: 10.1016/j.ydbio.2011.03.009.

[5] W. W. Branford and H. J. Yost, “Nodal Signaling: CrypticLefty Mechanism of Antagonism Decoded,” *Current Biology*, vol. 14, no. 9, pp. R341–R343, May 2004, doi: 10.1016/j.cub.2004.04.020.

[6] X. Zhou, L. Lowe, H. Sasaki, B. L. M. Hogan, and M. R. Kuehn, “Nodal is a novel TGF-β-like gene expressed in the mouse node during gastrulation,” *Nature*, vol. 361, no. 6412, pp. 543–547, Feb. 1993, doi: 10.1038/361543a0.

[7] Y. Chen and A. F. Schier, “Lefty Proteins Are Long-Range Inhibitors of Squint-Mediated Nodal Signaling,” *Current Biology*, vol. 12, no. 24, pp. 2124–2128, Dec. 2002, doi: 10.1016/S0960-9822(02)01362-3.

[8] C. Chen and M. M. Shen, “Two Modes by which Lefty Proteins Inhibit Nodal Signaling,” *Current Biology*, vol. 14, no. 7, pp. 618–624, Apr. 2004, doi: 10.1016/j.cub.2004.02.042.

[9] J. J. Essner, J. D. Amack, M. K. Nyholm, E. B. Harris, and H. J. Yost, “Kupffer’s vesicle is a ciliated organ of asymmetry in the zebrafish embryo that initiates left-right development of the brain, heart and gut,” *Development*, vol. 132, no. 6, pp. 1247–1260, Mar. 2005, doi: 10.1242/dev.01663.

[10] J. Gros, K. Feistel, C. Viebahn, M. Blum, and C. J. Tabin, “Cell Movements at Hensen’s Node Establish Left/Right Asymmetric Gene Expression in the Chick,” *Science*, vol. 324, no. 5929, pp. 941–944, May 2009, doi: 10.1126/science.1172478.

[11] P. Vick *et al.*, “Flow on the right side of the gastrocoel roof plate is dispensable for symmetry breakage in the frog Xenopus laevis,” *Developmental Biology*, vol. 331, no. 2, pp. 281–291, Jul. 2009, doi: 10.1016/j.ydbio.2009.05.547.

[12] S. Nonaka, H. Shiratori, Y. Saijoh, and H. Hamada, “Determination of left–right patterning of the mouse embryo by artificial nodal flow,” *Nature*, vol. 418, no. 6893, pp. 96–99, Jul. 2002, doi: 10.1038/nature00849.

[13] A. Schweickert *et al.*, “Cilia-Driven Leftward Flow Determines Laterality in Xenopus,” *Current Biology*, vol. 17, no. 1, pp. 60–66, Jan. 2007, doi: 10.1016/j.cub.2006.10.067.

[14] Y. Okada, S. Takeda, Y. Tanaka, J.-C. I. Belmonte, and N. Hirokawa, “Mechanism of Nodal Flow: A Conserved Symmetry Breaking Event in Left-Right Axis Determination,” *Cell*, vol. 121, no. 4, pp. 633–644, May 2005, doi: 10.1016/j.cell.2005.04.008.

[15] Y. Tanaka, Y. Okada, and N. Hirokawa, “FGF-induced vesicular release of Sonic hedgehog and retinoic acid in leftward nodal flow is critical for left–right determination,” *Nature*, vol. 435, no. 7039, pp. 172–177, May 2005, doi: 10.1038/nature03494.

[16] S. Nonaka *et al.*, “Randomization of Left–Right Asymmetry due to Loss of Nodal Cilia Generating Leftward Flow of Extraembryonic Fluid in Mice Lacking KIF3B Motor Protein,” *Cell*, vol. 95, no. 6, pp. 829–837, Dec. 1998, doi: 10.1016/S0092-8674(00)81705-5.

[17] P. Oteíza, M. Köppen, M. L. Concha, and C.-P. Heisenberg, “Origin and shaping of the laterality organ in zebrafish,” *Development*, vol. 135, no. 16, pp. 2807–2813, Aug. 2008, doi: 10.1242/dev.022228.

[18] M. S. Cooper and L. A. D’amico, “A Cluster of Noninvoluting Endocytic Cells at the Margin of the Zebrafish Blastoderm Marks the Site of Embryonic Shield Formation,” *Developmental Biology*, vol. 180, no. 1, pp. 184–198, Nov. 1996, doi: 10.1006/dbio.1996.0294.

[19] N. Hirokawa, Y. Tanaka, Y. Okada, and S. Takeda, “Nodal Flow and the Generation of Left-Right Asymmetry,” *Cell*, vol. 125, no. 1, pp. 33–45, Apr. 2006, doi: 10.1016/j.cell.2006.03.002.

[20] R. P. Harvey, “Links in the Left/Right Axial Pathway,” *Cell*, vol. 94, no. 3, pp. 273–276, Aug. 1998, doi: 10.1016/S0092-8674(00)81468-3.

[21] Y.-Y. Kim *et al.*, “Meteorin Regulates Mesendoderm Development by Enhancing Nodal Expression,” *PLoS ONE*, vol. 9, no. 2, p. e88811, Feb. 2014, doi: 10.1371/journal.pone.0088811.

[22] J. Nishino, K. Yamashita, H. Hashiguchi, H. Fujii, T. Shimazaki, and H. Hamada, “Meteorin: a secreted protein that regulates glial cell differentiation and promotes axonal extension,” *EMBO J*, vol. 23, no. 9, pp. 1998–2008, May 2004, doi: 10.1038/sj.emboj.7600202.

[23] M. Ramialison *et al.*, “Rapid identification of PAX2/5/8 direct downstream targets in the otic vesicle by combinatorial use of bioinformatics tools,” *Genome Biol*, vol. 9, no. 10, p. R145, 2008, doi: 10.1186/gb-2008-9-10-r145.

[24] J. R. Jørgensen *et al.*, “Cometin is a novel neurotrophic factor that promotes neurite outgrowth and neuroblast migration in vitro and supports survival of spiral ganglion

neurons in vivo," *Experimental Neurology*, vol. 233, no. 1, pp. 172–181, Jan. 2012, doi: 10.1016/j.expneurol.2011.09.027.

[25] T. G. Montague, J. A. Gagnon, and A. F. Schier, "Conserved regulation of Nodal-mediated left-right patterning in zebrafish and mouse," *Development*, vol. 145, no. 24, p. dev171090, Dec. 2018, doi: 10.1242/dev.171090.

[26] S. Long, N. Ahmad, and M. Rebagliati, "The zebrafish *nodal* -related gene *southpaw* is required for visceral and diencephalic left-right asymmetry," *Development*, vol. 130, no. 11, pp. 2303–2316, Jun. 2003, doi: 10.1242/dev.00436.

[27] J. Brennan, D. P. Norris, and E. J. Robertson, "Nodal activity in the node governs left-right asymmetry," *Genes Dev.*, vol. 16, no. 18, pp. 2339–2344, Sep. 2002, doi: 10.1101/gad.1016202.

[28] Y. Saijoh, S. Oki, S. Ohishi, and H. Hamada, "Left–right patterning of the mouse lateral plate requires Nodal produced in the node," *Developmental Biology*, p. 13, 2003, doi: 10.1016/s0012-1606(02)00121-5.

[29] J. L. Pelliccia, G. A. Jindal, and R. D. Burdine, "Gdf3 is required for robust Nodal signaling during germ layer formation and left-right patterning," *eLife*, vol. 6, p. e28635, Nov. 2017, doi: 10.7554/eLife.28635.

[30] M. Hojo *et al.*, "Right-elevated expression of charon is regulated by fluid flow in medaka Kupffer's vesicle: Left-right asymmetric expression of charon," *Development, Growth & Differentiation*, vol. 49, no. 5, pp. 395–405, Jun. 2007, doi: 10.1111/j.1440-169X.2007.00937.x.

[31] F. Gourronc, N. Ahmad, N. Nedza, T. Eggleston, and M. Rebagliati, "Nodal activity around Kupffer's vesicle depends on the T-box transcription factors notail and spadetail and on notch signaling," *Dev. Dyn.*, vol. 236, no. 8, pp. 2131–2146, Aug. 2007, doi: 10.1002/dvdy.21249.

[32] J. Alexander, M. Rothenberg, G. L. Henry, and D. Y. R. Stainier, "casanova Plays an Early and Essential Role in Endoderm Formation in Zebrafish," *Developmental Biology*, vol. 215, no. 2, pp. 343–357, Nov. 1999, doi: 10.1006/dbio.1999.9441.

[33] Y. Kikuchi *et al.*, "*casanova* encodes a novel Sox-related protein necessary and sufficient for early endoderm formation in zebrafish," *Genes Dev.*, vol. 15, no. 12, pp. 1493–1505, Jun. 2001, doi: 10.1101/gad.892301.

[34] M. A. El-Brolosy *et al.*, "Genetic compensation triggered by mutant mRNA degradation," *Nature*, vol. 568, no. 7751, pp. 193–197, Apr. 2019, doi: 10.1038/s41586-019-1064-z.

[35] J. D. Amack and H. J. Yost, "The T Box Transcription Factor No Tail in Ciliated Cells Controls Zebrafish Left-Right Asymmetry," *Current Biology*, vol. 14, no. 8, pp. 685–690, Apr. 2004, doi: 10.1016/j.cub.2004.04.002.

[36] T. Matsui, I. Hiroshi, and B. Yasumasa, “Cell collectivity regulation within migrating cell cluster during Kupffer’s vesicle formation in zebrafish,” *Frontiers in Cell and Developmental Biology*, vol. 3, p. 8, 2015, doi: 10.3389/fcell.2015.00027.

[37] C. B. Kimmel, W. W. Ballard, S. R. Kimmel, B. Ullmann, and T. F. Schilling, “Stages of embryonic development of the zebrafish,” *Developmental Dynamics*, vol. 203, no. 3, pp. 253–310, 1995, doi: 10.1002/aja.1002030302.

[38] H. Hashimoto *et al.*, “The Cerberus/Dan-family protein Charon is a negative regulator of Nodal signaling during left-right patterning in zebrafish,” *Development*, vol. 131, no. 8, pp. 1741–1753, Apr. 2004, doi: 10.1242/dev.01070.

[39] P. Sampaio *et al.*, “Left-Right Organizer Flow Dynamics: How Much Cilia Activity Reliably Yields Laterality?,” *Developmental Cell*, vol. 29, no. 6, pp. 716–728, Jun. 2014, doi: 10.1016/j.devcel.2014.04.030.

[40] J. J. Gokey, Y. Ji, H. G. Tay, B. Litts, and J. D. Amack, “Kupffer’s vesicle size threshold for robust left-right patterning of the zebrafish embryo: Size Threshold For KV Function,” *Dev. Dyn.*, vol. 245, no. 1, pp. 22–33, Jan. 2016, doi: 10.1002/dvdy.24355.

[41] K. de Bruin *et al.*, “Cellular Dynamics of EGF Receptor–Targeted Synthetic Viruses,” *Molecular Therapy*, vol. 15, no. 7, pp. 1297–1305, Jul. 2007, doi: 10.1038/sj.mt.6300176.

[42] R. O. Hynes, “Integrins: Versatility, modulation, and signaling in cell adhesion,” *Cell*, vol. 69, no. 1, pp. 11–25, Apr. 1992, doi: 10.1016/0092-8674(92)90115-S.

[43] A. J. Ablooglu, E. Tkachenko, J. Kang, and S. J. Shattil, “Integrin αV is necessary for gastrulation movements that regulate vertebrate body asymmetry,” *Development*, vol. 137, no. 20, pp. 3449–3458, Oct. 2010, doi: 10.1242/dev.045310.

[44] B. W. Bisgrove, J. J. Essner, and H. J. Yost, “Multiple pathways in the midline regulate concordant brain, heart and gut left-right asymmetry,” *Development*, vol. 127, no. 16, pp. 3567–3579, Aug. 2000, doi: 10.1242/dev.127.16.3567.

[45] L. Solnica-Krezel *et al.*, “Mutations affecting cell fates and cellular rearrangements during gastrulation in zebrafish,” *Development*, vol. 123, no. 1, pp. 67–80, Dec. 1996, doi: 10.1242/dev.123.1.67.

[46] E. Pulgar *et al.*, “Apical contacts stemming from incomplete delamination guide progenitor cell allocation through a dragging mechanism,” *eLife*, vol. 10, p. e66483, Aug. 2021, doi: 10.7554/eLife.66483.

[47] R. Milner, G. Edwards, C. Streuli, and C. ffrench-Constant, “A Role in Migration for the αvβ1 Integrin Expressed on Oligodendrocyte Precursors,” *J Neurosci*, vol. 16, no. 22, pp. 7240–7252, Nov. 1996, doi: 10.1523/JNEUROSCI.16-22-07240.1996.

[48] B. Felding-Habermann *et al.*, “A Single Immunoglobulin-like Domain of the Human Neural Cell Adhesion Molecule L1 Supports Adhesion by Multiple Vascular and Platelet Integrins,”

Journal of Cell Biology, vol. 139, no. 6, pp. 1567–1581, Dec. 1997, doi: 10.1083/jcb.139.6.1567.

[49] M. R. Reboll *et al.*, “Meteorin-like promotes heart repair through endothelial KIT receptor tyrosine kinase,” *Science*, vol. 376, no. 6599, pp. 1343–1347, Jun. 2022, doi: 10.1126/science.abn3027.

[50] Y.-W. Dai *et al.*, “Meteorin links the bone marrow hypoxic state to hematopoietic stem/progenitor cell mobilization,” *Cell Reports*, vol. 40, no. 12, p. 111361, Sep. 2022, doi: 10.1016/j.celrep.2022.111361.

[51] E. M. Mellgren and S. L. Johnson, “kitb, a second zebrafish ortholog of mouse Kit,” *Dev Genes Evol*, vol. 215, no. 9, pp. 470–477, Sep. 2005, doi: 10.1007/s00427-005-0001-3.

[52] S. Zheng, Z. Li, J. Song, J. Liu, and C. Miao, “Metrnl: a secreted protein with new emerging functions,” *Acta Pharmacol Sin*, vol. 37, no. 5, pp. 571–579, May 2016, doi: 10.1038/aps.2016.9.

[53] W. Y. Hwang *et al.*, “Efficient genome editing in zebrafish using a CRISPR-Cas system,” *Nat Biotechnol*, vol. 31, no. 3, pp. 227–229, Mar. 2013, doi: 10.1038/nbt.2501.

[54] C. Thisse and B. Thisse, “High-resolution in situ hybridization to whole-mount zebrafish embryos,” *Nat Protoc*, vol. 3, no. 1, pp. 59–69, Jan. 2008, doi: 10.1038/nprot.2007.514.

[55] A. Streit and C. D. Stern, “Combined Whole-Mount in Situ Hybridization and Immunohistochemistry in Avian Embryos,” *Methods*, vol. 23, no. 4, pp. 339–344, Apr. 2001, doi: 10.1006/meth.2000.1146.

[56] R. Tang, A. Dodd, D. Lai, W. C. McNabb, and D. R. Love, “Validation of Zebrafish (Danio rerio) Reference Genes for Quantitative Real-time RT-PCR Normalization,” *ABBS*, vol. 39, no. 5, pp. 384–390, May 2007, doi: 10.1111/j.1745-7270.2007.00283.x.

[57] M. Valcu and C.-M. Valcu, “Data transformation practices in biomedical sciences,” *Nat Methods*, vol. 8, no. 2, pp. 104–105, Feb. 2011, doi: 10.1038/nmeth0211-104.

[58] A. Borovina, S. Superina, D. Voskas, and B. Ciruna, “Vangl2 directs the posterior tilting and asymmetric localization of motile primary cilia,” *Nat Cell Biol*, vol. 12, no. 4, Art. no. 4, Apr. 2010, doi: 10.1038/ncb2042.

[59] I. F. Sbalzarini and P. Koumoutsakos, “Feature point tracking and trajectory analysis for video imaging in cell biology,” *Journal of Structural Biology*, vol. 151, no. 2, pp. 182–195, 2005, doi: 10.1016/j.jsb.2005.06.002.

[60] N. Tarantino *et al.*, “TNF and IL-1 exhibit distinct ubiquitin requirements for inducing NEMO–IKK supramolecular structures,” *Journal of Cell Biology*, vol. 204, no. 2, pp. 231–245, Jan. 2014, doi: 10.1083/jcb.201307172.

[61] A. Dereeper *et al.*, “Phylogeny.fr: robust phylogenetic analysis for the non-specialist,” *Nucleic Acids Res*, vol. 36, no. Web Server issue, pp. W465–W469, Jul. 2008, doi: 10.1093/nar/gkn180.

[62] A. Dereeper, S. Audic, J.-M. Claverie, and G. Blanc, “BLAST-EXPLORER helps you building datasets for phylogenetic analysis,” *BMC Evol Biol*, vol. 10, p. 8, Jan. 2010, doi: 10.1186/1471-2148-10-8.

[63] R. C. Edgar, “MUSCLE: multiple sequence alignment with high accuracy and high throughput,” *Nucleic Acids Res*, vol. 32, no. 5, pp. 1792–1797, 2004, doi: 10.1093/nar/gkh340.

[64] J. Castresana, “Selection of Conserved Blocks from Multiple Alignments for Their Use in Phylogenetic Analysis,” *Molecular Biology and Evolution*, vol. 17, no. 4, pp. 540–552, Apr. 2000, doi: 10.1093/oxfordjournals.molbev.a026334.

[65] S. Guindon and O. Gascuel, “A Simple, Fast, and Accurate Algorithm to Estimate Large Phylogenies by Maximum Likelihood,” *Systematic Biology*, vol. 52, no. 5, pp. 696–704, Oct. 2003, doi: 10.1080/10635150390235520.

[66] M. Anisimova and O. Gascuel, “Approximate Likelihood-Ratio Test for Branches: A Fast, Accurate, and Powerful Alternative,” *Systematic Biology*, vol. 55, no. 4, pp. 539–552, Aug. 2006, doi: 10.1080/10635150600755453.

[67] F. Chevenet, C. Brun, A.-L. Bañuls, B. Jacq, and R. Christen, “TreeDyn: towards dynamic graphics and annotations for analyses of trees,” *BMC Bioinformatics*, vol. 7, p. 439, Oct. 2006, doi: 10.1186/1471-2105-7-439.

Acknowledgements

We thank all members of the Del Bene lab for discussions, the Institut Curie and Institut de la Vision imaging and animal facilities. We acknowledge the lab of Jean Livet for their support with the chick analysis. We would like to thank Pierre Luc Bardet from IBPS (Sorbonne Université) for fruitful discussions. We thank Clémence Gentner from Gilles Tessier’s lab at the Institut de la Vision for the microspheres sample. Work in the Del Bene laboratory was supported by ANR MetAxon [ANR-17-CE16-0007], the IHU FOReSIGHT [ANR-18-IAHU-0001], CNRS, INSERM, and Sorbonne Université core funding. F.E. was supported by the École des Neurosciences de Paris (ENP) Ile-de-France network and the Fondation pour la Recherche Médicale (FRM). F.D.S. was supported by a doctoral fellowship of the Curie International PhD program. T.O.A. was supported by a Boehringer Ingelheim Fonds PhD Fellowship.

Authors contribution

F.E. did the experimental work and analyzed the results. L.B. contributed to the experimental works. F.D.S., T.A and K.D. generated the CRISPR/Cas9 *metrn* mutant lines. J.B.W performed the KV microbeads tracking analysis. F.E, S.A. and F.D.B. conceived the project and wrote

the manuscript. S.A. and F.D.B. co-supervised the study. All the authors reviewed and edited the manuscript.

Ethics declarations

Competing interests

The authors declare no competing interests.